PERGAMON

International Journal of Mechanical Sciences 42 (2000) 487–502

International Journal of MECHANICAL SCIENCES

www.elsevier.com/locate/ijmecsci

Tooth contact analysis of face-gear drives

Shuo-Hung Chang[a,*], Tsang-Dong Chung[b], Shui-Shong Lu[a]

[a]*Department of Mechanical Engineering, National Taiwan University, Taipei, Taiwan, Republic of China*
[b]*Department of Mechanical Engineering, Nanya Junior College, Chung-Li 320, Taiwan, Republic of China*

Received 9 March 1998; received in revised form 5 January 1999

Abstract

Based on the face-gear generation process, the analytical geometry of the face-gear drive and its mathematical model for tooth contact analysis of the face-gear and the spur pinion meshing were derived. The tooth contact paths and the transmission errors due to assembly error along the axis of face-gear, misalignment of crossed and angular displacements between axes of spur pinion and face-gear were analyzed. Furthermore, the conditions of undercutting and pointing in the generation process were studied. Several design charts were then developed. Finally, the conditions of undercutting and pointing for a face-gear drive were all identified in meshing with and without assembly error along the direction of the axis of face-gear and misalignment of angular displacement between axes of spur pinion and face-gear. Several numerical examples were also presented.

Keywords: Face-gear; Tooth contact analysis; Kinematic error; Undercutting; Pointing

1. Introduction

Face-gears have been widely used in low-power transmission applications. An important application of a face-gear drive is in a helicopter transmission [1,6] as shown in Fig. 1.

It uses the idea of the split torque that appears to be significant where a spur pinion drives two face-gears to provide an accurate division of power. This mechanism greatly reduces the size and cost compared to conventional design.

* Corresponding author. Tel.: 886-2-2363-3863; fax: 886-2-2363-1755.
E-mail address: shchang@ccms.ntu.edu.tw (S.H. Chang)

0020-7403/00/$ - see front matter
PII: S0020-7403(99)00013-2

Nomenclature

a_g addendum of the face-gear
D shortest distance between the axes of x_a and z_f in coordinate systems of S_a and S_f
KE kinematic error
$\mathbf{L}_{ij}$ transformation matrices which transform the vectors from coordinate system S_j to S_i
L_1 inner radius of face-gear out of undercutting in the generation process
L_1' inner radius of face-gear out of undercutting during meshing of the face-gear drive
L_2 outer radius of face-gear free of pointing in the generation process
L_2' outer radius of face-gear free of pointing during meshing of the face-gear drive
m_{ij} gear ratio of N_j to N_i
$\mathbf{M}_{ij}$ homogeneous transformation matrices which transform the vectors from coordinate system S_j to S_i
N_i number of teeth of shaper, spur pinion and face-gear for $i = s, 1, 2$
$\mathbf{n}_f^{(i)}$ unit normal of the spur pinion and face-gear tooth surfaces represented in the coordinate system S_f $(i = 1, 2)$
$\mathbf{R}_f^{(i)}$ position vectors of the spur pinion and face-gear tooth surfaces represented in the coordinate system S_f $(i = 1, 2)$
r_{as} addendum circle radius of the shaper
r_{b1} base circle radius of the spur pinion
r_{bs} base circle radius of the shaper
r_{p1} pitch circle radius of the spur pinion
r_{ps} pitch circle radius of the shaper
$\mathbf{r}_i$ position vectors of the shaper, spur pinion and face-gear for $i = s, 1, 2$
S_i coordinate system S $(i = 1, 2, a, b, c, f, m, s, t)$
u_1 Gaussian coordinate of Σ_1
u_s Gaussian coordinate of Σ_s
$\mathbf{v}_s^{(s2)}$ sliding velocity between shaper and face-gear
α instant pressure angle in the generation process
α_0 pressure angle of the shaper
ΔE shortest distance between the spur pinion and the face-gear axes
$\Delta\gamma$ angular misalignment of the face-gear
Δp assembly error along the axis of the face-gear
φ_i rotational angle of shaper, spur pinion and face-gear for $i = s, 1, 2$
θ_1 Gaussian coordinate of Σ_1
θ_0 the width of spur pinion teeth on the base circle
θ_{os} the width of shaper teeth on the base circle
θ_s Gaussian coordinate of Σ_s
γ half-shaft angle of face-gear
γ_f half-cone angle of face-gear including angular misalignment
γ_m half-cone angle of face-gear
Σ_i tooth surface of spur pinion, face-gear and shaper $(i = 1, 2, s)$
ω_i rotational speed of shaper, spur pinion and face-gear $(i = s, 1, 2)$
$\boldsymbol{\omega}_s^{(i)}$ rotation speed of shaper, spur pinion and face-gear $(i = s, 1, 2)$ in coordinate system S_s

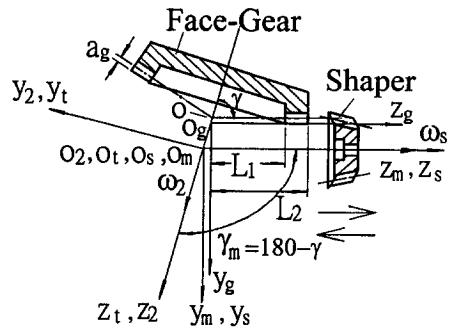

Fig. 1. Face-gear generation process.

Until now, there were few research activities about manufacture and design of face-gear drive. Buckingham [2] and Dudley [3] provided a brief description of face-gear drives. The research about face-gear drives was initiated by McDonnell Douglas Helicopter Co. Important investigations of face-gear drives have been performed by Litvin [1,6] and Litvin et al. [4,5]. However, the papers mentioned above did not yet study the misalignment effects on kinematic error of face-gear drives, undercutting and pointing problems.

In this paper we include the following sections. (1) Generation process of the face-gear. The face-gear tooth surface can be derived by the coordinate transformation and meshing equation of the shaper. (2) Kinematics of the face-gear meshing with the spur pinion. The tooth surface vectors of the face-gear and the spur pinion are both transformed to the fixed coordinate system S_f. (3) Tooth contact analysis and kinematic errors. Numerical analysis is performed for contact path and transmission errors induced by assembly errors along axis of face-gear direction and by misalignment of the crossed and angular displacements between axes of face-gear and spur pinion. (4) Undercutting and pointing. While designing a face-gear, it is important to avoid pointing and undercutting of the face-gear. Effects of pressure angle and tooth number of the shaper on undercutting and pointing of the face-gear are studied. (5) Numerical results and discussion. (6) Conclusion. The analysis is limited to the case of face-gear drives with the intersecting axes.

2. Generation process of the face-gear

The generation process of a face-gear by a shaper is illustrated in Fig. 1. The face-gear and the shaper rotate about their own axes with angular velocities ω_2 and ω_s, respectively. Both axes intersect at the point O_m. Coordinate systems $S_s(x_s, y_s, z_s)$, $S_2(x_2, y_2, z_2)$ and $S_m(x_m, y_m, z_m)$, are, respectively, fixed on the shaper, face-gear, and the frame of cutting machine.

The face-gear tooth surface, Σ_2, is determined as the envelope to the family of shaper surface, Σ_s, represented in coordinate system S_s. The shaper surface, Σ_s, and its position vector, $\mathbf{r}_s$,

are related by [4,6]

$$\mathbf{r}_s(u_s,\theta_s) = \begin{bmatrix} r_{bs}[\sin(\theta_{os}+\theta_s) - \theta_s\cos(\theta_{os}+\theta_s)] \\ -r_{bs}[\cos(\theta_{os}+\theta_s) + \theta_s\sin(\theta_{os}+\theta_s)] \\ u_s \\ 1 \end{bmatrix}, \tag{1}$$

where u_s and θ_s are surface coordinates of the shaper, r_{bs} is the base circle radius of the shaper, θ_{os} determines the width of the shaper space on the base circle and can be represented by the equation

$$\theta_{os} = \frac{\pi}{2N_s} - inv\,\alpha_0, \tag{2}$$

where N_s and α_o are tooth number and pressure angle of the shaper, respectively, and *inv* is the involute function. The unit normal $\mathbf{n}_s$ to the shaper surface is given by

$$\mathbf{n}_s = \frac{\dfrac{\partial \mathbf{r}_s}{\partial \theta_s} \times \dfrac{\partial \mathbf{r}_s}{\partial u_s}}{\left|\dfrac{\partial \mathbf{r}_s}{\partial \theta_s} \times \dfrac{\partial \mathbf{r}_s}{\partial u_s}\right|} = -\begin{bmatrix} \cos(\theta_{os}+\theta_s) \\ \sin(\theta_{os}+\theta_s) \\ 0 \end{bmatrix}. \tag{3}$$

We represent the face-gear tooth surface, Σ_2, in coordinate system S_2 by the following matrix equation:

$$\mathbf{r}_2(u_s, \theta_s, \varphi_s) = \mathbf{M}_{2s}\,(\varphi_s)\mathbf{r}_s(u_s, \theta_s), \tag{4}$$

where $\mathbf{M}_{2s}$ is the homogeneous transformation matrix from coordinate system S_s to S_2 given in appendix. The auxiliary coordinate system $S_t(x_t, y_t, z_t)$ in Fig. 2 is set up to facilitate the coordinate transformation. The angle γ_m between axes z_m and z_2 is determined by $\gamma_m = 180 - \gamma$, where γ is the half-shaft angle of the face-gear. The rotational angles of the face-gear, φ_{2t} and the shaper, φ_s, are related by $\varphi_{2t} = \varphi_s N_s/N_2$ where N_2 and N_s denote the tooth numbers of the face-gear and the shaper, respectively. The equation of meshing is represented as Eqs. (5) and (6) [1,6]. Such

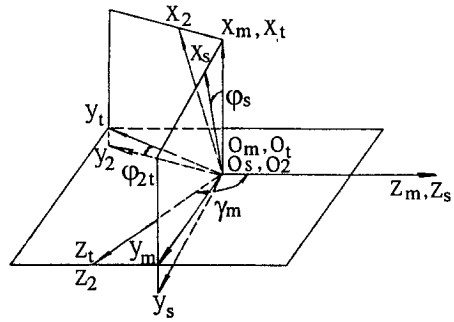

Fig. 2. Coordinate system S_s, S_m, S_2 and S_t applied for generation.

equations insure that the generating and the generated gear tooth surfaces are always in tangency during the generating process. Due to the tangency of two mating surfaces, the relative velocity of the surfaces must be on the common tangent plane.

$$\mathbf{n}_s \cdot \mathbf{v}_s^{(s2)} = f(u_s, \theta_s, \varphi_s) = 0, \tag{5}$$

$$\mathbf{v}_s^{(s2)} = (\boldsymbol{\omega}_s^{(s)} - \boldsymbol{\omega}_s^{(2)}) \times \mathbf{r}_s, \tag{6}$$

where $\mathbf{v}_s^{(s2)}$, $\boldsymbol{\omega}_s^{(s)}$ and $\boldsymbol{\omega}_s^{(2)}$ denote, respectively, the sliding velocity between shaper and face-gear, angular velocities of shaper and face-gear in coordinate system S_s. From Eqs. (4)–(6), parameter u_s can be eliminated, so that the position vector for the tooth surface of the face-gear can be represented as a function of θ_s and φ_s.

3. Kinematics of face-gear meshing with spur pinion

The tooth surfaces are represented by Σ_i, $i = 1$ for pinion and 2 for face-gear. In computer simulation, it is assumed that there are misalignment of crossed and angular displacements between two rotating axes of the mating gears. Also assembly error is assume to exist along the axis of face-gear direction.

Coordinate systems $S_1(x_1, y_1, z_1)$ and $S_f(x_f, y_f, z_f)$ are fixed on the spur pinion and the frame of the face-gear drive as shown in both Figs. 3 and 4(a) respectively. The coordinate system S_1 can be transformed to the coordinate system S_f by rotating the coordinate about axis z_1 or z_f through an angle φ_1. In order to simulate the misalignment of the face-gear, auxiliary coordinate systems $S_a(x_a, y_a, z_a)$, $S_b(x_b, y_b, z_b)$ and $S_c(x_c, y_c, z_c)$ are set up in Fig. 4(b). The location of S_a with respect to S_f is shown in Fig. 4(a). Parameters $\Delta E, D$ and $D\cot\gamma$ determine the location of the origin O_a with respect to O_f, where ΔE denotes the crossed displacement that is the shortest distance between the spur pinion and the face-gear axes when the axes are crossed but not intersected. In the alignment meshing, $\Delta E = 0$ that is the spur pinion and the face-gear axes intersect. In the following analysis, ΔE is used to simulate the misalignment of the crossed displacement between axes of spur pinion and face-gear. The crossed angle, $\gamma_f = 180 - \gamma + \Delta\gamma$, is used to simulate the angular misalignment

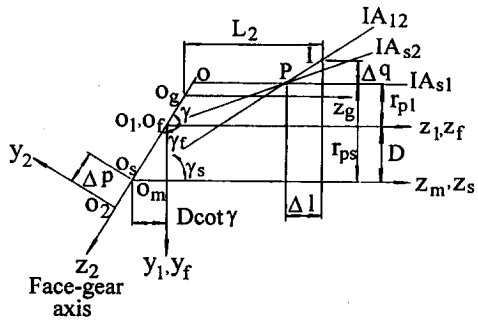

Fig. 3. Relationship of coordinate systems of shaper, spur opinion and face-gear.

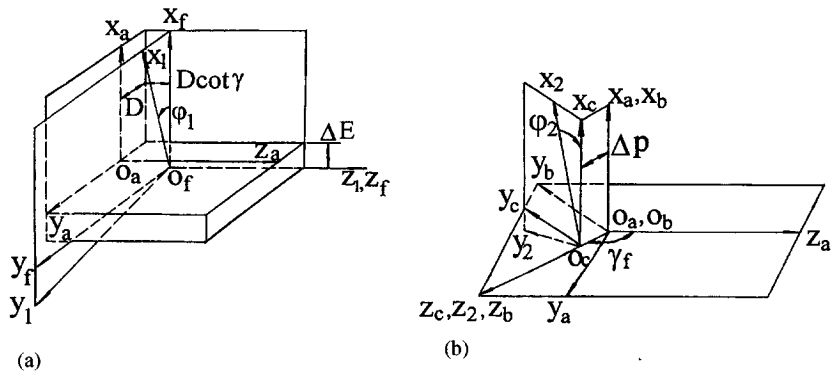

Fig. 4. (a) Relationship of coordinate system S_a, S_1 and S_f; (b) Relationship of coordinate system S_2, S_a, S_b and S_c.

of S_b with respect to S_a. $\Delta\gamma$ is caused by the misalignment of angular displacement between axes of spur pinion and face-gear. The variable Δp along the axis of face-gear, also shown in both Figs. 3 and 4(b), represents the misalignment of S_c with respect to S_b that simulates the assembly error of the face-gear along its rotating axis, z_c. The coordinate system S_2 can be transformed to the coordinate system S_c by rotating axis z_2 through an angle φ_2. The face-gear rotates about the axis z_2 as shown in both Figs. 3 and 4(b).

According to Figs. 3 and 4(a), the equation of the spur pinion tooth surface can be represented in the fixed coordinate system S_f by applying the following coordinate transformation matrix equation:

$$\mathbf{R}_f^{(1)} = \mathbf{M}_{f1}\mathbf{r}_1, \tag{7}$$

where $\mathbf{r}_1$ is position vector of the spur pinion surface similar to $\mathbf{r}_s$ in Eq. (1) except subscript s is replaced by 1. Matrix $\mathbf{M}_{f1}$ is the homogeneous transformation matrix from coordinate system S_1 to S_f. u_1, θ_1 and r_{b1} denote the surface coordinates and base circle radius of the spur pinion, respectively. θ_o determines the width of the spur pinion space on the base circle and can be represented similarly to the equation (2) except N_s is replaced by N_1. N_1 denotes tooth numbers of the spur pinion. The unit normal $\mathbf{n}_1$ to the spur pinion surface is similar to Eq. (3) except subscript s is replaced by 1. It can be expressed in coordinate system S_f as

$$\mathbf{n}_f^{(1)} = \mathbf{L}_{f1}\mathbf{n}_1, \tag{8}$$

where $\mathbf{L}_{f1}$ is the transformation matrix from coordinate system S_1 to S_f.

According to Figs. 1, 4(a) and (b), the equations for the tooth surface of the face-gear and its unit normal can, respectively, be represented in the fixed coordinate system S_f by

$$\mathbf{R}_f^{(2)} = \mathbf{M}_{f2}\mathbf{M}_{2s}\mathbf{r}_s \tag{9}$$

and

$$\mathbf{n}_f^{(2)} = \mathbf{L}_{f2}\mathbf{L}_{2s}\mathbf{n}_s. \tag{10}$$

$\mathbf{M}_{f2}$ and $\mathbf{L}_{f2}$ are, respectively, the homogeneous transformation matrix and the transformation matrix from coordinate system S_2 to S_f. $\mathbf{M}_{2s}$ and $\mathbf{L}_{2s}$ are the homogeneous transformation matrix

and the transformation matrix from coordinate system S_s to S_2, respectively. See the appendix for details on all the homogeneous transformation matrices and the transformation matrices.

4. Tooth contact analysis and kinematic error

In order to perform the tooth contact analysis (TCA), the equations of face-gear and spur pinion tooth surfaces should be represented in the fixed coordinate system S_f. At any instant, the spur pinion meshes with the face-gear in point contact [4,6]. At the point of contact, due to the tangency of the two gear tooth surfaces, the position vectors and their unit normals of both the face-gear and spur pinion tooth surfaces should be the same. Therefore, the following equations can be observed [4,6]:

$$\mathbf{R}_f^{(1)} = \mathbf{R}_f^{(2)}, \tag{11}$$

$$\mathbf{n}_f^{(1)} = \mathbf{n}_f^{(2)}. \tag{12}$$

Eqs. (11), (12) and with relationship of $|\mathbf{n}_f^{(1)}| = |\mathbf{n}_f^{(2)}| = 1$ form a system of five independent equations with six unknowns: φ_2, φ_1, θ_1, u_1, θ_s and φ_s. φ_l and φ_2 denote the rotational angles of spur pinion and face-gear, respectively. One of the unknowns, φ_2, may be considered as input variable to solve the five independent equations with five unknowns.

As φ_2 is chosen as the input variable in practical operation, φ_1 is then the output rotational angle. However, for ideal gear meshing, the output rotational angle, $\varphi_1 = \varphi_2 N_1/N_2$, where N_1 and N_2 denote the number of teeth of spur pinion and face-gear, respectively. From the derivation above, the relation between φ_1 and φ_2 is a nonlinear function in practical case. The kinematic error of the gear train can be expressed as

$$\Delta\varphi_1 = \varphi_1 - \varphi_2 N_1/N_2, \tag{13}$$

where $\Delta\varphi_1$ represents the kinematic error of the gear train as a function of input variable φ_2.

5. Undercutting and pointing

It is necessary to avoid undercutting and pointing of the teeth of the face-gear in the design of a face-gear drive. The undercutting of the generated teeth will be developed near the root area when interference between the shaper and the generated gear occurs. It means that the generated surface is not always in tangency with the generating tool surface. The pointing of the teeth means that the tooth thickness on the top of the tooth becomes zero. They both make the strength of the teeth weak. Undercutting and pointing can be avoided by proper dimensions of the inner and outer radii of the face-gear. In this section, we will consider the problems of undercutting and pointing of the face-gear during generation and spur pinion meshes with face-gear.

5.1. Undercutting and pointing of the face-gear during generation

The general conditions of avoiding undercutting can be found from the works of Litvin [1,6] and Litvin et al. [4,5]. During the generation process of the face-gear surface, Σ_2, by a shaper,

appearance of singular points on Σ_2 is a warning that the surface may be undercut. In the generation process, the mathematical definition of singularity of Σ_2 may be represented by the equation, $\mathbf{v}_r^{(2)} = 0$, that yields $\mathbf{v}_r^{(s)} + \mathbf{v}^{(s2)} = 0$, where $\mathbf{v}_r^{(2)}$ and $\mathbf{v}_r^{(s)}$ denote, respectively, the velocities of the contact point on face-gear and shaper with respect to the coordinate system S_s and $\mathbf{v}^{(s2)}$ denotes the sliding velocity between Σ_s and Σ_2.

Combining equation $\mathbf{v}_r^{(s)} + \mathbf{v}^{(s2)} = 0$ and differentiated equation of meshing,

$$\frac{\mathrm{d}}{\mathrm{d}t}[f(u_s, \theta_s, \varphi_s)] = 0 \tag{14}$$

allow one to find singular points at any rotational angle φ_s of shaper on Σ_2. By connecting singular points allows one to determine a line L which would to divide the shaper tooth surface to two regions. Solution exists for Eq. (14), if the following conditions are satisfied:

$$\Delta_1 = \begin{vmatrix} \dfrac{\partial x_s}{\partial u_s} & \dfrac{\partial x_s}{\partial \theta_s} & v_{xs}^{(s2)} \\ \dfrac{\partial y_s}{\partial u_s} & \dfrac{\partial y_s}{\partial \theta_s} & v_{ys}^{(s2)} \\ f_{us} & f_{\theta s} & f_{\varphi s}\dfrac{\mathrm{d}\varphi_s}{\mathrm{d}t} \end{vmatrix} = 0, \tag{15}$$

$$\Delta_2 = \begin{vmatrix} \dfrac{\partial x_s}{\partial u_s} & \dfrac{\partial x_s}{\partial \theta_s} & v_{xs}^{(s2)} \\ \dfrac{\partial z_s}{\partial u_s} & \dfrac{\partial z_s}{\partial \theta_s} & v_{zs}^{(s2)} \\ f_{us} & f_{\theta s} & f_{\varphi s}\dfrac{\mathrm{d}\varphi_s}{\mathrm{d}t} \end{vmatrix} = 0 \tag{16}$$

and

$$\Delta_3 = \begin{vmatrix} \dfrac{\partial y_s}{\partial u_s} & \dfrac{\partial y_s}{\partial \theta_s} & v_{ys}^{(s2)} \\ \dfrac{\partial z_s}{\partial u_s} & \dfrac{\partial z_s}{\partial \theta_s} & v_{zs}^{(s2)} \\ f_{us} & f_{\theta s} & f_{\varphi s}\dfrac{\mathrm{d}\varphi_s}{\mathrm{d}t} \end{vmatrix} = 0. \tag{17}$$

$v_{xs}^{(s2)}$, $v_{ys}^{(s2)}$ and $v_{zs}^{(s2)}$ denote the components of the relative velocities at the point of contact between shaper and face-gear in the coordinate system S_s which can be obtained from Eq. (6). The solution of simultaneous system of Eqs. (15)–(17) is the singular point (u_s,θ_s) on the shaper surface for rotational angle φ_s. A sufficient condition for singularity of Σ_2 can be represented by

$$\Delta_1^2 + \Delta_2^2 + \Delta_3^2 = F(u_s, \theta_s, \varphi_s) = 0. \tag{18}$$

A simple way to avoid singularity and undercutting of the face-gear surface, Σ_2, is to solve [1,6]

$$f(u_s, \theta_s, \varphi_s) = 0, \quad F(u_s, \theta_s, \varphi_s) = 0. \tag{19}$$

With the relation of $\mathbf{r}_s = \mathbf{r}_s(u_s, \theta_s)$ given in Eq. (1), simultaneous Eq. (19) can be solved to determine a line L_1 which defines the undercutting limit on the generating surface. Similarly, the undercutting limit line on the generated face-gear can also be derived by transformation from coordinate system S_s to S_2.

In Fig. 3, The location of the tooth pointing is at the point I. Point P in the figure is the pitch point. The maximum radius L_2 which will limit the tooth length to avoid pointing on the face-gear can be determined by

$$L_2 = r_{ps}(1/\tan\gamma_s - 1/\tan\gamma) + a_g/\tan\gamma + \Delta 1, \tag{20}$$

where

$$\Delta 1 = \frac{r_{ps}}{\tan\gamma_s}\left(\frac{\cos\alpha_0 - \cos\alpha}{\cos\alpha}\right). \tag{21}$$

γ_s and a_g denote half-pitch cone angle of the shaper and addendum of the face-gear, respectively, and α is the instant pressure angle during generation.

5.2. *Undercutting and pointing of the face-gear meshing with spur pinion*

During the spur pinion meshes with the face-gear, the mathematical definition of singularity of Σ_2 are same as Eqs. (14)–(19) except the subscript s is replaced by 1. With the relation of $\mathbf{r}_1 = \mathbf{r}_1(u_1, \theta_1)$, simultaneous Eq. (19) where the subscript s is replaced by 1 can be solved to determine a line L_1' with which defines the undercutting limit of the spur pinion surface. Similarly, the undercutting limit line on the generated face-gear can also be derived by transformation from coordinate system S_1 to S_2.

The maximum radius L_2' which will limit the tooth length to avoid pointing on the face-gear can be determined by Eqs. (20) and (21) except the subscript s is replaced by 1.

6. Numerical results and discussion

The analysis of tooth contact paths, kinematic errors, undercutting and pointing of face-gear drives are presented in this section. In the following numerical examples, pressure angle of spur pinion, face-gear and shaper is 25°, the tooth number of spur pinion, face-gear and shaper are 28, 107 and 31, respectively, and the pitch cone angle of the face-gear is 160°. We will limit the analysis to the case of face-gear drives with intersecting axes. Numerical examples are given below to illustrate the effects of various conditions of gear meshing on the tooth contact path, kinematic error, the undercutting and pointing.

In Table 1, we consider the displacement of contact point for aligned face-gear drive with intersecting axes and for misalignment of $\Delta E = 0.1$ mm between axes of face-gear and spur pinion. The effect of positive value of ΔE is to bring the contact points closer to the inner radius and the root of the face-gear teeth. It leads to less torque driving upon the gear sets and a larger load capacity for the face-gear. Displaced bearing contacts due to assembly error, Δp, and misalignment of angular displacement, $\Delta\gamma$, are shown in Table 1 as well. The effects of positive Δp and $\Delta\gamma$ just

Table 1
Contact paths of ideal case, $\Delta E = 0.1$ (mm), $\Delta p = 0.1$ (mm) and $\Delta\gamma = 0.01$ (deg.)

Diff. case	Ideal case			$\Delta E = 0.1$ (mm)		
φ_2 (deg)	x_f (mm)	y_f (mm)	z_f (mm)	x_f (mm)	y_f (mm)	z_f (mm)
1.5	5.49	− 42.506	192.463	5.516	− 42.299	188.249
1.0	4.182	− 42.986	199.625	4.199	− 42.755	194.62
0.5	2.874	− 43.467	208.256	2.881	− 43.207	202.191
0	1.565	− 43.947	218.529	1.563	− 43.659	211.278
− 0.5	0.256	− 44.424	230.796	0.245	− 44.111	222.16
− 1.0	− 1.053	− 44.901	245.588	− 1.074	− 44.564	235.229
− 1.5	− 2.363	− 45.378	263.496	− 2.393	− 45.013	250.895
	$\Delta p = 0.1$ (mm)			$\Delta\gamma = 0.01$(deg)		
φ_2 (deg)	x_f (mm)	y_f (mm)	z_f (mm)	x_f (mm)	y_f (mm)	z_f (mm)
1.5	5.727	− 43.003	204.809	5.579	− 42.709	197.287
1.0	4.446	− 43.55	214.435	4.285	− 43.227	205.656
0.5	3.163	− 44.095	225.881	2.994	− 43.75	215.791
0	1.88	− 44.64	239.656	1.704	− 44.279	228.11
− 0.5	0.598	− 45.185	256.341	0.417	− 44.812	243.084
− 1.0	− 0.685	− 45.728	276.611	− 0.866	− 45.356	261.671
− 1.5	− 1.969	− 46.27	301.663	− 2.144	− 45.914	285.088

show opposite to that of positive ΔE. It results in a larger torque on the gear sets and more bending for the teeth of the face-gear.

The effects of misalignment of angular displacement, $\Delta\gamma$, and the assembly error, Δp, along the axis of the face-gear on the undercutting and pointing were also calculated when the spur pinion meshes with the face-gear. Table 2 shows the inner radius L_1' to avoid undercutting and outer radius L_2' to avoid pointing of face-gear for various $\Delta\gamma$ and Δp. It shows that larger misalignment of angular displacement results in a larger inner radius to avoid undercutting and larger outer radius to avoid pointing of the face-gear. A larger assembly error, Δp, along the axis of face-gear leads to smaller inner radius to avoid undercutting and smaller outer radius to avoid pointing of the face-gear.

Kinematic errors due to misalignment ΔE between axes of spur pinion and face-gear as functions of input rotational angle are shown in Fig. 5. In this particular gear meshing, the spur pinion and face-gear will contact at input angle, φ_2, from 1.6° to − 1.6°. In the negative rotational part (0 to 1.6°), larger misalignment ΔE leads to a larger kinematic error. In the positive rotational part (1.6 to 0°), kinematic error is relatively insensitive to misalignment. Kinematic errors due to misalignment Δp along the rotational axis of the face-gear direction as functions of input rotational angle are shown in Fig. 6. In the negative rotational part, larger misalignment Δp leads to a larger kinematic error. In the positive rotational part, there is less effect on kinematic error due to larger

Table 2
Inner radius to avoid undercutting and outer radius to avoid pointing of face-gear with respect to different misalignment of angular displacement between axes of spur pinion and face-gear and different assembly error along the axis of the face-gear direction

Pressure angle α_0 (deg)	$\Delta\gamma = 0.01$ (deg) $\Delta p = 0.0$ (mm) L_1' (mm)	L_2' (mm)	$\Delta\gamma = 0.03$ (deg) $\Delta p = 0.0$ (mm) L_1' (mm)	L_2' (mm)	$\Delta\gamma = 0.05$ (deg) $\Delta p = 0.0$ (mm) L_1' (mm)	L_2' (mm)
25.0	156.0737	194.0157	156.0828	194.0308	156.0910	194.0459
22.5	159.2568	195.4317	159.2665	195.4470	159.2761	195.4623
20.0	162.1221	196.4710	162.1325	196.4864	162.1489	196.5019
17.5	164.6630	197.2017	164.6738	197.2173	164.6748	197.2329
14.5	167.2733	197.7481	167.2864	197.7638	167.2982	197.7794
	$\Delta p = 0.05$ (mm) $\Delta\gamma = 0.0$ (deg)		$\Delta p = 0.1$ (mm) $\Delta\gamma = 0.0$ (deg)		$\Delta p = 0.2$ (mm) $\Delta\gamma = 0.0$ (deg)	
α_0 (deg)	L_1' (mm)	L_2' (mm)	L_1' (mm)	L_2' (mm)	L_1' (mm)	L_2' (mm)
25.0	156.0520	189.0918	156.0377	184.1754	156.0091	174.3427
22.5	159.2070	190.4718	159.1927	185.5194	159.1641	175.6147
20.0	162.0860	191.4845	162.0717	186.5057	162.0431	176.5482
17.5	164.6315	192.1966	164.6172	187.1993	164.5886	177.2046
14.5	167.2490	192.7291	167.2347	187.7179	167.2061	177.6954

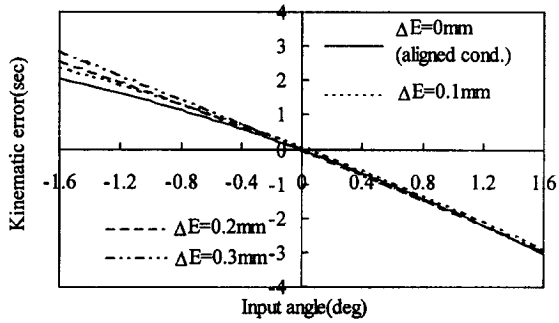

Fig. 5. Effect of crossed displacement between axes of spur pinion and face-gear on kinematic errors.

value of Δp. Kinematic errors due to angular misalignment, $\Delta\gamma$, as functions of input rotational angle are shown in Fig. 7. In the negative rotational part, larger misalignment $\Delta\gamma$ leads to a larger kinematic error. In the positive rotational part, larger assembly error leads to a smaller kinematic error.

Fig. 8 shows the boundary lines between undercutting and non-undercutting regions for a given pressure angle of shaper and an inner radius of module 3.175 mm under different shaper tooth number. For non-undercutting meshing, it shows that smaller pressure angle of the shaper would require larger inner radius of the generated face-gear.

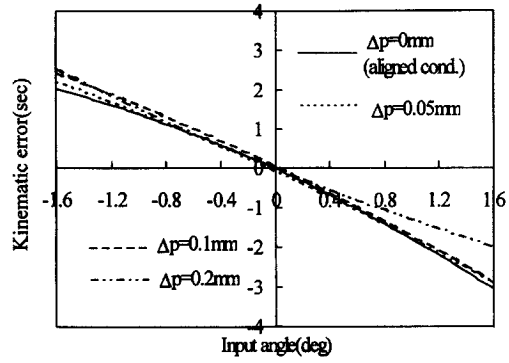

Fig. 6. Effect of displacement in the direction of rotation axis of face-gear on kinematic error.

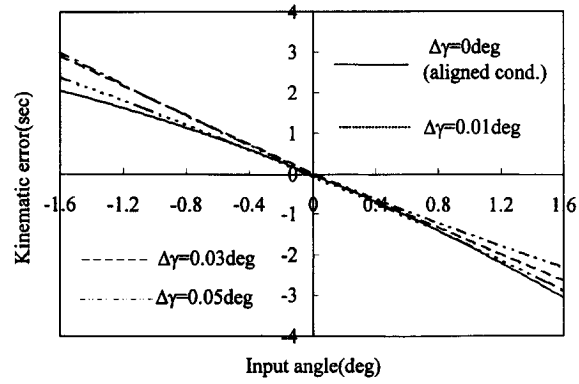

Fig. 7. Effect of misalignment of angular displacement between axes of spur pinion and face-gear on kinematic errors.

Fig. 9 shows the boundary lines between pointing and non-pointing regions for a given outer radius of the face-gear and a pressure angle of the shaper as functions of tooth number of the shaper. For non-pointing meshing, a less tooth number and a larger pressure angle of the shaper require a smaller outer radius of the generated face-gear.

7. Conclusions

From the numerical examples discussed above, some important characteristics of this type of face-gear drive are listed as follows:

1. The effect of positive ΔE leads to the less torque driving upon the gear sets and the larger load capacity for the face-gear. The effect of positive of Δp or $\Delta \gamma$ just shows the opposite consequence.

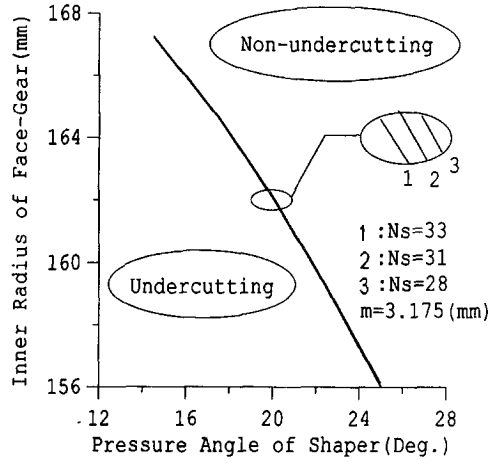

Fig. 8. Undercutting conditions in different tooth number of shaper.

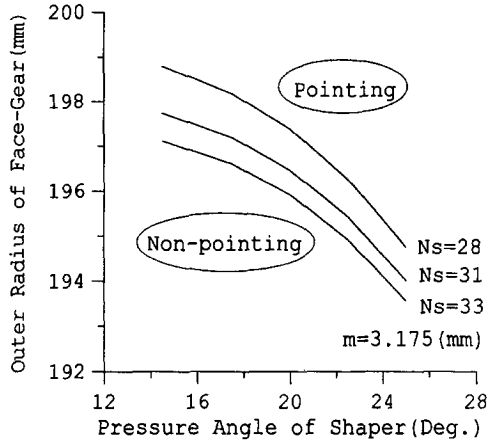

Fig. 9. Pointing conditions in different tooth number of shaper.

2. Larger misalignment of angular displacement, $\Delta\gamma$, leads to larger inner and outer radii of the face-gear to avoid undercutting and pointing, respectively. The effects are just opposite due to assembly error, Δp, along the axis of the face-gear.
3. Kinematic error is insensitive to the assembly error along axis of the face-gear direction, misalignment of crossed and angular displacement between axes of spur pinion and face-gear in this type of face-gear drive.
4. When the tooth number of shaper increases, the dimensions of inner radius free of undercutting and outer radius to avoid pointing of the generated face-gear are smaller.
5. The developed design charts provide the undercutting and pointing conditions in the generation and meshing processes.

Appendix A

1. Homogeneous transformation matrices $\mathbf{M}_{2s}$, $\mathbf{M}_{2t}$, $\mathbf{M}_{tm}$, $\mathbf{M}_{ms}$ and transformation matrices $\mathbf{L}_{2s}$, $\mathbf{L}_{2t}$, $\mathbf{L}_{tm}$, $\mathbf{L}_{ms}$.

$\mathbf{M}_{2s}$ is the homogeneous transformation matrix from coordinate system S_s to S_2 expressed by the following

$$\mathbf{M}_{2s} = \mathbf{M}_{2t}\mathbf{M}_{tm}\mathbf{M}_{ms}, \tag{A.1}$$

where

$$\mathbf{M}_{ms} = \begin{bmatrix} \cos\varphi_s & -\sin\varphi_s & 0 & 0 \\ \sin\varphi_s & \cos\varphi_s & 0 & 0 \\ 0 & 0 & 1 & 0 \\ 0 & 0 & 0 & 1 \end{bmatrix}, \tag{A.2}$$

$$\mathbf{M}_{tm} = \begin{bmatrix} 1 & 0 & 0 & 0 \\ 0 & \cos\gamma_m & -\sin\gamma_m & 0 \\ 0 & \sin\gamma_m & \cos\gamma_m & 0 \\ 0 & 0 & 0 & 1 \end{bmatrix}, \tag{A.3}$$

$$\mathbf{M}_{2t} = \begin{bmatrix} \cos\varphi_{2t} & \sin\varphi_{2t} & 0 & 0 \\ -\sin\varphi_{2t} & \cos\varphi_{2t} & 0 & 0 \\ 0 & 0 & 1 & 0 \\ 0 & 0 & 0 & 1 \end{bmatrix}. \tag{A.4}$$

$\mathbf{M}_{ms}$, $\mathbf{M}_{tm}$ and $\mathbf{M}_{2t}$ are the homogeneous coordinate transformation matrices from S_s to S_m, S_m to S_t, S_t to S_2, respectively, as seen in Figs. 1 and 2. Matrices $\mathbf{L}_{2s}$, $\mathbf{L}_{2t}$, $\mathbf{L}_{tm}$ and $\mathbf{L}_{ms}$, are the corresponding rotational submatrices of $\mathbf{M}_{2s}$, $\mathbf{M}_{2t}$, $\mathbf{M}_{tm}$ and $\mathbf{M}_{ms}$, respectively.

2. Homogeneous transformation matrices $\mathbf{M}_{f1}$ and transformation matrices $\mathbf{L}_{f1}$.

$\mathbf{M}_{f1}$ is the homogeneous transformation matrix from coordinate system S_1 to S_f given by

$$\mathbf{M}_{fl} = \begin{bmatrix} \cos\varphi_1 & \sin\varphi_1 & 0 & 0 \\ -\sin\varphi_1 & \cos\varphi_1 & 0 & 0 \\ 0 & 0 & 1 & 0 \\ 0 & 0 & 0 & 1 \end{bmatrix}, \tag{A.5}$$

$\mathbf{L}_{f1}$ is the corresponding rotational submatrice of $\mathbf{M}_{f1}$.

3. Homogeneous transformation matrices $\mathbf{M}_{f2}$, $\mathbf{M}_{fa}$, $\mathbf{M}_{ab}$, $\mathbf{M}_{bc}$, $\mathbf{M}_{c2}$, and transformation matrices $\mathbf{L}_{f2}$, $\mathbf{L}_{fa}$, $\mathbf{L}_{ab}$, $\mathbf{L}_{bc}$, $\mathbf{L}_{c2}$.

$\mathbf{M}_{f2}$ is the homogeneous transformation matrix from coordinate system S_2 to S_f. $\mathbf{M}_{c2}$, $\mathbf{M}_{bc}$, $\mathbf{M}_{ab}$, $\mathbf{M}_{fa}$ are the homogeneous matrices from coordinate systems S_2 to S_c, S_c to S_b, S_b to S_a and S_a to S_f, respectively, as seen in Figs. 4(a) and (b).

$$\mathbf{M}_{f2} = \mathbf{M}_{fa}\mathbf{M}_{ab}\mathbf{M}_{bc}\mathbf{M}_{c2}, \tag{A.6}$$

where

$$\mathbf{M}_{c2} = \begin{bmatrix} \cos\varphi_2 & -\sin\varphi_2 & 0 & 0 \\ \sin\varphi_2 & \cos\varphi_2 & 0 & 0 \\ 0 & 0 & 1 & 0 \\ 0 & 0 & 0 & 1 \end{bmatrix}, \tag{A.7}$$

$$\mathbf{M}_{bc} = \begin{bmatrix} 1 & 0 & 0 & 0 \\ 0 & 1 & 0 & 0 \\ 0 & 0 & 1 & \Delta p \\ 0 & 0 & 0 & 1 \end{bmatrix}, \tag{A.8}$$

$$\mathbf{M}_{ab} = \begin{bmatrix} 1 & 0 & 0 & 0 \\ 0 & \cos\gamma_f & -\sin\gamma_f & 0 \\ 0 & \sin\gamma_f & \cos\gamma_f & 0 \\ 0 & 0 & 0 & 1 \end{bmatrix}, \tag{A.9}$$

$$\mathbf{M}_{fa} = \begin{bmatrix} 1 & 0 & 0 & D \\ 0 & 1 & 0 & \Delta E \\ 0 & 0 & 1 & -D\cot\gamma \\ 0 & 0 & 0 & 1 \end{bmatrix}. \tag{A.10}$$

Matrices $\mathbf{L}_{f2}$, $\mathbf{L}_{fa}$, $\mathbf{L}_{ab}$, $\mathbf{L}_{bc}$, and $\mathbf{L}_{c2}$ are the corresponding rotational submatrices of the homogeneous matrices $\mathbf{M}_{f2}$, $\mathbf{M}_{fa}$, $\mathbf{M}_{ab}$, $\mathbf{M}_{bc}$ and $\mathbf{M}_{c2}$, respectively.

References

[1] Litvin FL. Theory of gearing. Washington DC: NASA Publication RP-1212, 1989.
[2] Buckingham E. Analytical mechanics of gears. New York: Dover, 1949.
[3] Dudley DW. Gear handbook. The design, manufacture, and application of gears. New York: McGraw-Hill, 1962.
[4] Litvin FL, Zhang Y, Wang JC, Bossler RB, Chen JD. Design and geometry of face-gear drives. ASME Transactions Journal of Mechanical Design. 1992;114:642–7.

[5] Litvin FL, Wang JC, Bossler RB, Chen JD, Heath G. David G. Application of face-gear drives in helicopter transmissions. Proceedings of the International Power Transmission and Gearing Conference, ASME, vol. 1, 1992: 267–74.
[6] Litvin FL. Gear geometry and applied theory. Englewood Cliffs, NJ: Prentice-Hall, 1994:490–525.